MATERIALS CHEMISTRY FRONTIERS

RESEARCH ARTICLE

View Article Online
View Journal | View Issue

Cite this: *Mater. Chem. Front.*, 2023, **7**, 735

Reducing non-radiative voltage losses in organic solar cells using molecular encapsulation†

Anirudh Sharma, ‡[a] Lisa Sharma,‡[b] Jules Bertrandie,[a] Diego R. Villalva,[a] Yajun Gao,[a] Catherine S. P. De Castro,[a] Joel Troughton,[a] Julien Gorenflot,[a] Frederic Laquai,[a] Hugo Bronstein *[b] and Derya Baran*[a]

Received 11th October 2022,
Accepted 14th December 2022

DOI: 10.1039/d2qm01044e

rsc.li/frontiers-materials

Non-radiative voltage loss is one of the significant bottlenecks limiting the performance of organic solar cells (OSCs). This work presents a material design approach for conjugated polymers isolating the polymer chains with molecular encapsulation, enabling better control over the donor–acceptor spacing. Bulk-heterojunction OSCs based on encapsulated polymers as electron donors show a remarkable increase of ∼50 mV in the V_{oc}. Significant improvement in the V_{oc} is attributed to reduced non-radiative voltage losses as evidenced by enhanced electroluminescence as a result of suppressed intermolecular aggregation and an increase in structural disorder. Importantly, molecular encapsulation resulted in notable improvement in the operational stability of OSCs with no burn-in loss in V_{oc}, presenting a promising strategy to simultaneously enhance the performance and operational stability of OSCs.

Introduction

Organic solar cells (OSCs) witnessed tremendous progress in the last two decades,[1] now achieving power conversion efficiencies (PCEs) of up to 19% for single-junction devices.[2,3] The PCE of OSCs is limited mainly by the open-circuit voltage (V_{oc}), often lower than the optical bandgap ($E_{g\,opt}$), mainly due to non-radiative charge recombination. As per the Shockley–Queisser model, an ideal solar cell should also be an ideal light-emitting diode (LED), having only radiative recombination (100% electroluminescence external quantum efficiency EQE_{EL}).[4,5] However, in actual devices, non-radiative recombination simultaneously takes place, which is relatively more predominant in OSCs than inorganic counterparts.[6]

In most OSCs, EQE_{EL} is very low typically on the order of $\sim 10^{-6}$–10^{-4}, resulting in total energy loss ΔE_{loss} ($E_{g\,opt} - qV_{oc}$) of ∼500–600 meV, with non-radiative voltage loss (ΔV_{ocnr}) being the key loss mechanism,[7–9] and is expressed as:

$$\Delta V_{ocnr} = -\frac{kT}{q}\ln(EQE_{EL}) \quad (1)$$

where k is the Boltzmann constant, T is the temperature, and q is the electronic charge. Thus, it is clear that significantly reducing the (ΔV_{ocnr})[10] is essential to minimize ΔE_{loss} and to achieve OSCs with PCEs of 20% and above. New material design strategies are urgently required to develop photoactive materials with enhanced photoluminescence and electroluminescence yields.[11,12]

So far, the rapid progress in the development of OSCs can be attributed mainly to the design and synthesis of new materials, primarily focusing on minimizing the voltage losses,[10,12] and tuning the optical bandgap and frontier molecular orbital energies.[13–16] Nevertheless, besides optimizing the energetic offsets, material design strategies are still needed to intrinsically limit the (ΔV_{ocnr}) that occur due to the recombination of the photo-generated charges.

Conjugated push–pull polymers based on electron-deficient lactam core of diketopyrrolopyrrole (DPP) have found a wide range of applications for optoelectronic devices,[17] owing to their good electronic properties, photochemical stability, and industrial relevance. However, due to a planar backbone, DPP polymers have been found to have a strong tendency to aggregate, which can limit the performance of OSCs *via* geminate charge recombination.[18] Furthermore, polymer aggregates, for example, are known to result in the formation of non-emissive charge transfer states,[19] limiting the device performance. Wang *et al.* have recently demonstrated that by increasing the donor–acceptor (DA) spacing, V_{oc} of OSCs can be improved *via* reduced non-radiative decay of charge carriers.[20]

Covalently attached molecular encapsulation previously reported by Sugiyasu,[21] Pan,[22] and others has been shown to

[a] *KAUST Solar Center (KSC), Physical Sciences and Engineering Division (PSE), King Abdullah University of Science and Technology (KAUST), Thuwal, 23955, Kingdom of Saudi Arabia. E-mail: derya.baran@kaust.edu.sa*
[b] *Department of Chemistry and Physics, University of Cambridge, Lensfield Road, Cambridge CB2 1EW, UK. E-mail: hab60@cam.ac.uk*

† Electronic supplementary information (ESI) available. CCDC 2164409 and 2177219. For ESI and crystallographic data in CIF or other electronic format see DOI: https://doi.org/10.1039/d2qm01044e

‡ A.S. and L.S. contributed equally

reduce π–π stacking interactions in conjugated polymers by isolating the polymer chains, significantly improving the emissivity of the polymers.[23] However, due to the reduction/elimination of π–π interactions, which would likely result in reduced charge-carrier mobility, encapsulated conjugated polymers have rarely been successfully implemented into optoelectronic devices.

In this study, we use DPP-based polymers as the model system to demonstrate the reduction of (ΔV_{ocnr}) in OSCs. This is achieved by tuning the morphological and optoelectronic properties of polymers utilizing molecular encapsulation.[23] We utilize a half-encapsulated approach to modulate the properties of thiophene-flanked DPP-based conjugated polymer. By only protecting a single face of a monomer unit and additionally introducing it at a low concentration into a non-encapsulated host polymer, we aim to maintain sufficient bulk charge carrier mobility whilst improving the luminescence efficiency of a BHJ OSC and hence reduce the (ΔV_{ocnr}). We selected narrow bandgap polymer PDPP-TT, first synthesized by Li *et al.*,[24] due to its good performance in OSCs and high solubility. Here, new analogs of this polymer were synthesized by systematically incorporating varying amounts of half-encapsulated DPP monomer units into the polymer backbone. Encapsulation of the DPP core resulted in a notable enhancement of V_{oc} by 50 mV *via* reduced(ΔV_{ocnr}). Molecular encapsulation reduced polymer aggregation, enhancing the electroluminescence in polymer:$PC_{71}BM$ OSCs. Importantly, no changes were observed in the ionization energy of the polymers as a result of molecular encapsulation, presenting a promising molecular strategy to reduce (ΔV_{ocnr}), without the need to design completely new molecules. This promising molecular design strategy can be implemented to a variety of existing π-conjugated systems and be used with alternative non-fullerene acceptors.

Results and discussion

The synthesis of the half-encapsulated monomer is shown in Scheme 1, and its detailed procedure is described in the ESI.† The synthesis of the encapsulated DPP monomer began with the di-alkylation of **1** (DPP) using 1,10-dibromodecane in DMF and K_2CO_3 as the base. Compound **1** (DPP) was prepared *via* a method previously reported in the literature.[25] In order to minimize the production of the competing side products, including mono- and di-alkylated DPP, a solution of the alkyl chain in DMF underwent slow dropwise addition to a largely diluted basic solution of **1**. Upon workup, the crude material was purified *via* column chromatography, followed by sonication in hexane. The pure product was then collected *via* filtration to give **2** as a bright pink solid (16%). Finally, **2** underwent di-bromination with NBS at 50 °C to afford **3** as a dark purple solid (79%) (Scheme 1). The structure of compound **3**, was determined by X-ray crystallographic analysis (single crystals grown from $CHCl_3$:MeOH, Fig. 1),[26] confirming the successful encapsulation of the DPP core. The X-ray structure of **2** was also obtained and can be found in the ESI† (Fig. S1). The successful half-encapsulation can clearly be seen, and the molecule retains a co-planar conformation. However, slight bending of the DPP core can be seen, suggesting some strain may have been introduced through encapsulation.

Monomer **4** was synthesized based on previously reported literature.[27] The reference polymer, PDPP-TTref, (which contains no encapsulated monomer) was synthesized *via* a Stille cross-coupling between monomer **4** and 2,5-bis(trimethylstannyl)-thieno[3,2-*b*]thiophene, based on a procedure by Heeger *et al.*[27] (Scheme 2). The polymer then underwent Soxhlet extraction using acetone, hexane and dichloromethane to afford PDPP-TTref at a 77% yield. The new encapsulated polymers, PDPP-TT5%, PDPP-TT10%, and PDPP-TT20%, were then synthesized by incorporating an increasing ratio of monomer **3** in the place of monomer **4** (Table 1), using the same procedure used to synthesize PDPP-TTref, where the term *x*% reflects the feed ratio of the encapsulated monomer in the polymer. The polymers were then purified *via* Soxhlet extraction as before and isolated in either dichloromethane (DCM), chlorobenzene (CB), or chloroform ($CHCl_3$). The monomer ratios, molecular weights, and polydispersity index (PDI) of the polymers in the study are summarized in Table 1.

The thin-film absorption spectra of PDPP-TTref, as well as of its analogs with varying amounts of encapsulated units, are shown in Fig. 2a. For PDPP-TTref, the absorption peak was found to be at 821 nm, and blue-shifted when increasing the fraction of encapsulated units in the polymer backbone. For all polymer analogs, a blue shift in the absorption was also observed in the solution (Fig. 2b), suggesting reduced aggregation with the introduction of encapsulated units in the polymer backbone. Alternatively, the slight bending of the DPP chromophore as observed in the X-ray structure may have resulted in a slight loss of conjugation along the polymer backbone.

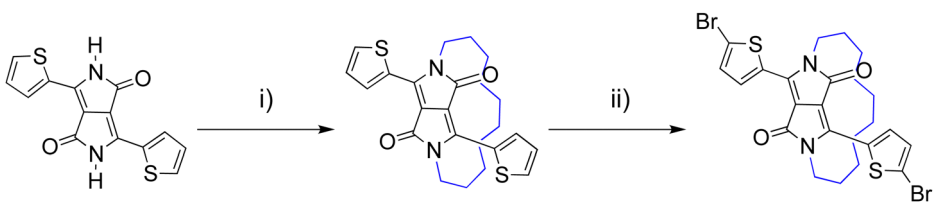

1 **2** 16 % **3** 79 %

Scheme 1 Synthesis of encapsulated DPP monomer **3** (i) 1,10-dibromodecane, K_2CO_3, 18-crown-6, DMF, 120 °C, 18 h; (ii) NBS, $CHCl_3$, 50 °C, 5 h.

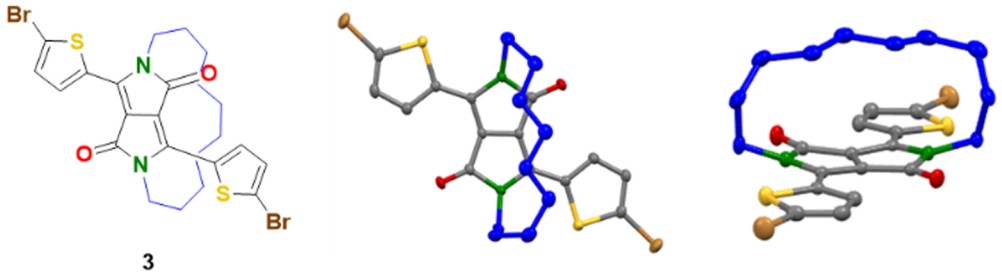

Fig. 1 Crystal structure of encapsulated monomer **3** (forward and side perspective view). Crystals grown from $CHCl_3$:MeOH.

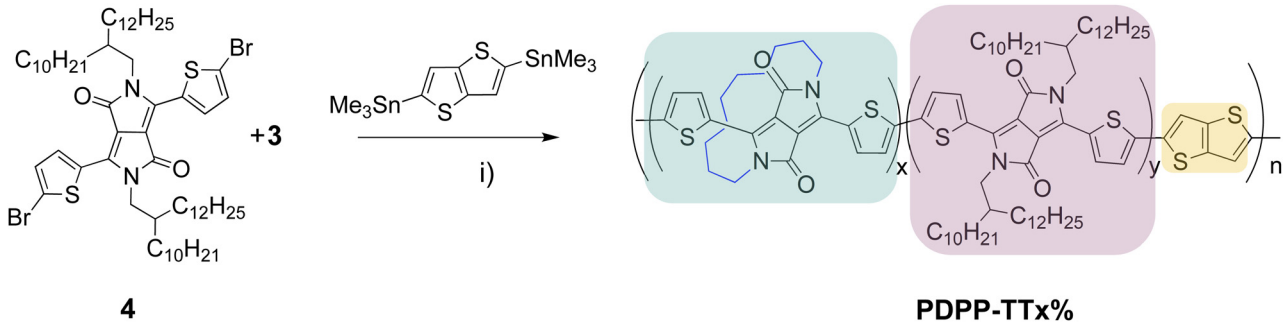

Scheme 2 Synthesis of encapsulated DPP polymers.

Table 1 Properties of encapsulated conjugated polymers

	Monomer ratio			Molecular weight[a]		
Polymer	**4**	**3**	TT	M_n (g mol^{-1})	M_w (g mol^{-1})	PDI
PDPP-TTref	1	0	1	26.3 K	102.7 K	3.9
PDPP-TT5%	0.95	0.05	1	24.4 K	79.1 K	3.2
PDPP-TT10%	0.90	0.1	1	78.4 K	221.2 K	2.8
PDPP-TT20%	0.80	0.2	1	14.0 K	76.4 K	5.5

[a] Determined by gel permeation chromatography (GPC) in CB against polystyrene (PS) standard.

The photovoltaic properties of OSCs fabricated with an active layer based on different polymer analogs and $PC_{71}BM$ BHJ blends are shown in Fig. 2 and summarized in Table 2. OSCs based on PDPP-TTref demonstrated a modest PCE of 2.8% with a V_{oc} of 0.64 V, which remained unchanged for PDPP-TT5% devices. However, devices based on PDPP-TT10% demonstrated a significantly enhanced V_{oc} of 0.69 V, resulting in the highest PCE of 6.1%. It is worth noting that in the case of PDPP-TT20% devices, a drop of 40 mV was observed in the V_{oc}, compared to the PDPP-TT10% devices. The statistical distribution of device parameters can be found in Fig. S17 (ESI†). Though all devices exhibited a broad spectral response, the EQE of the PDPP-TT10% and PDPP-TT20% devices were found to be significantly higher between ~650–850 nm resulting in enhanced J_{sc}, as compared to the devices based on the PDPP-TTref and PDPP-TT5% donor polymers (Fig. 2e). This is potentially due to the increase in the donor–acceptor intermixing owing to the expected reduction in molecular packing in the polymer phase, leading to better extraction of the photogenerated charges.

To verify the enhancement of V_{oc} with molecular encapsulation in the polymer backbone, analogs of another DPP-based polymer, PDPP-P, were also synthesized.[18] OSCs based on PDPP-P:$PC_{71}BM$ BHJ blends also showed an improvement of ~30 mV in the V_{oc} when encapsulated units were incorporated into the polymer backbone (Fig. S18 and Table S4, ESI†).

To understand the improvement in the V_{oc} upon molecular encapsulation of the donor polymer, we first studied possible changes in the ionization energy (IE) and electron affinity (EA) of DPP-TT polymer analogs using ultraviolet photoelectron spectroscopy (UPS) and low-energy inverse photoelectron spectroscopy (LE-IPES).[14] For PDPP-TTref, IE and EA were measured to be 5.16 eV and 3.38 eV (Fig. 3), respectively, corresponding to a transport gap of 1.78 eV. Though the IE of all-polymer analogs was found to be similar within the experimental uncertainties (~0.05 eV) (PDPP-TT5% – 5.12 eV, PDPP-TT10% – 5.14 eV, PDPP-TT20% – 5.17 eV), the EA of PDPP-TT5%, PDPP-TT10%, and PDPP-TT20% were measured to be 3.48 eV, 3.46 eV, and 3.29 eV, respectively (Fig. 3c). From the frontier molecular orbital energies measured using UPS and LE-IPES, a similar photovoltaic gap (ΔE_{pv}) between the highest occupied molecular orbital (HOMO) of all polymer analogs and the lowest occupied molecular orbital (LUMO) of the electron acceptor material in this case $PC_{71}BM$, is expected. Thus, the observed enhancement in the device V_{oc} upon molecular encapsulation of the polymer is independent of the material's energetics.

Detailed electrical and photo-physical characterization of PDPP-TT: $PC_{71}BM$ devices were further performed for an

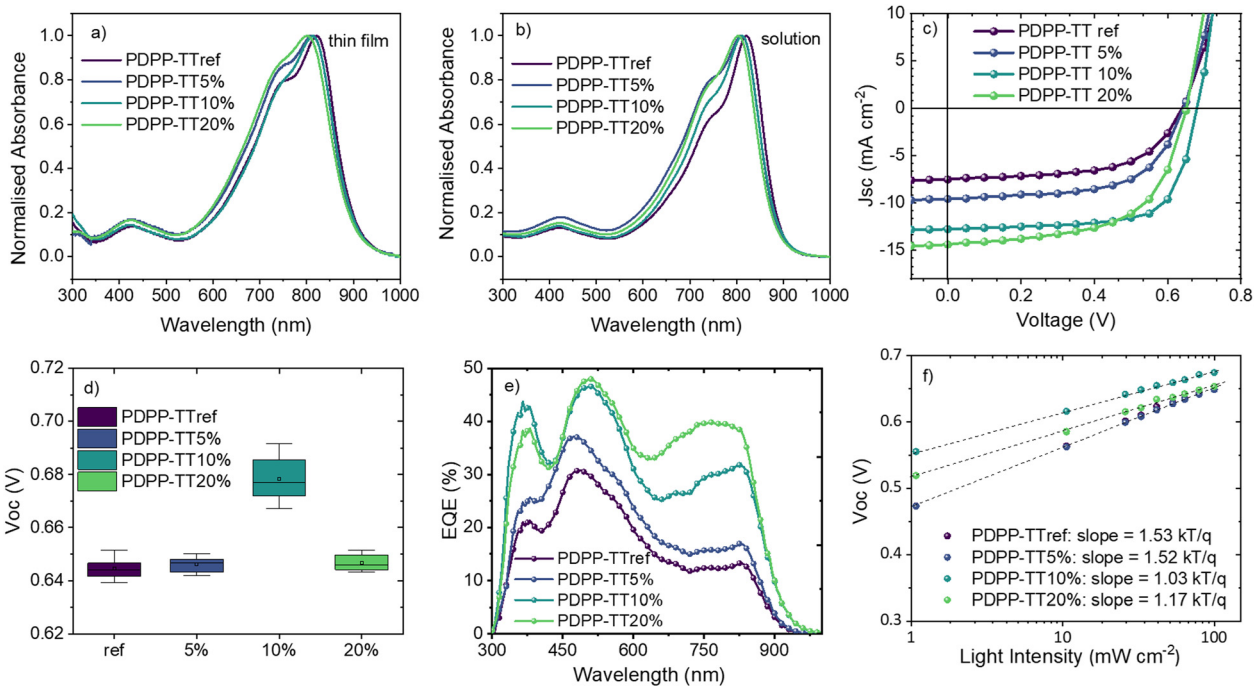

Fig. 2 Normalized UV-Vis absorption spectra of different PDPP-TT polymer analogs in (a) thin films (spin-coated from 5 mg mL^{-1} in CB) and (b) solutions (CB). (c) *J*–*V* characteristics, (d) box-plot depicting the statistical distribution of V_{oc}, (e) EQE, and (f) intensity-dependent V_{oc} measurements for OSCs with different PDPP-TT donor polymer analogs.

Table 2 Summary of *J*–*V* parameters, optical bandgap $E_{g\,opt}$, Urbach energy (E_u), V_{oc} loss of OSCs fabricated using donor polymers based on PDPP-TT analogs with varying fraction of the encapsulated units. The average PCE values are calculated over six devices

PDPP-TT	J_{sc} (mA cm^{-2})	V_{oc} (V)	FF (%)	PCE_{avg} (%)	PCE_{max} (%)	$E_{g\,opt}$ (eV)	E_u (meV)	$e\Delta V_{oc}$ (eV)	V_{ocrad} (V)	ΔV_{ocnr} (V)
Ref	7.5	0.64	58	2.7	2.8	1.43	34.11 ± 0.61	0.79	1.05	0.41
5%	9.6	0.64	61	3.6	3.8	1.43	40.33 ± 0.44	0.79	1.05	0.41
10%	12.8	0.69	69	6.0	6.1	1.42	38.90 ± 0.22	0.73	1.04	0.35
20%	14.4	0.65	59	5.5	5.6	1.42	40.91 ± 0.26	0.77	1.03	0.38

insightful understanding of the V_{oc} trend. First, the charge recombination mechanisms were probed by measuring *J*–*V* characteristics at different light intensities. J_{sc} and V_{oc} plotted against the natural logarithm of the light intensity provide information about the bimolecular and trap-assisted recombination, respectively.[28] Light intensity-dependent V_{oc} measurements show that when 10% encapsulated units are introduced within the polymer backbone, trap-assisted recombination is significantly reduced, as evident from the calculated slope of 1.53 kTq^{-1} and 1.03 kTq^{-1} for PDPP-TTref and PDPP-TT10%, respectively (Fig. 2f). For PDPP-TT20%, the slope slightly increased to 1.17 kTq^{-1} compared to PDPP-TT10%. The above results suggest that a 10% fraction of encapsulated units within the polymer backbone results in an optimum intra and intermolecular order, thus facilitating efficient charge generation and transport. This results in the least trap-assisted charge recombination and explains the higher V_{oc} of 0.69 V and FF of 69% for the PDPP-TT10% devices (Table 2). The relatively higher trap-assisted recombination in the case of PDPP-TT20% devices suggests that even though the relatively higher amount of encapsulated fraction in PDPP-TT20% increases the donor–acceptor intermixing (*via* reduced aggregation in the polymer chains), in this case, the further increased encapsulation has a detrimental impact on the device performance, as reflected by the reduced FF.[29] On the other hand, the calculated slope of J_{sc} *vs.* the natural logarithm of light intensity for various polymer analogs saw a non-significant increase when encapsulated, suggesting little change in the bimolecular recombination (Fig. S17, ESI†).

In order to probe the disorder in the BHJ films when molecular encapsulation is introduced into the polymer backbone, sub-bandgap absorption was measured using photothermal deflection spectroscopy (PDS) (Fig. 4a and Table 2). Below the bandgap, a characteristic single exponential Urbach tail was observed,[30] which can be fitted according to eqn (2), where α is the material's absorption coefficient, E, the photon energy, E_u the Urbach energy, and E_c and A are material constants:

$$\alpha = A \times \exp\left(\frac{E - E_c}{E_u}\right) \quad (2)$$

For the PDPP-TTref-based BHJ blend, E_u of 34.11 ± 0.61 meV was

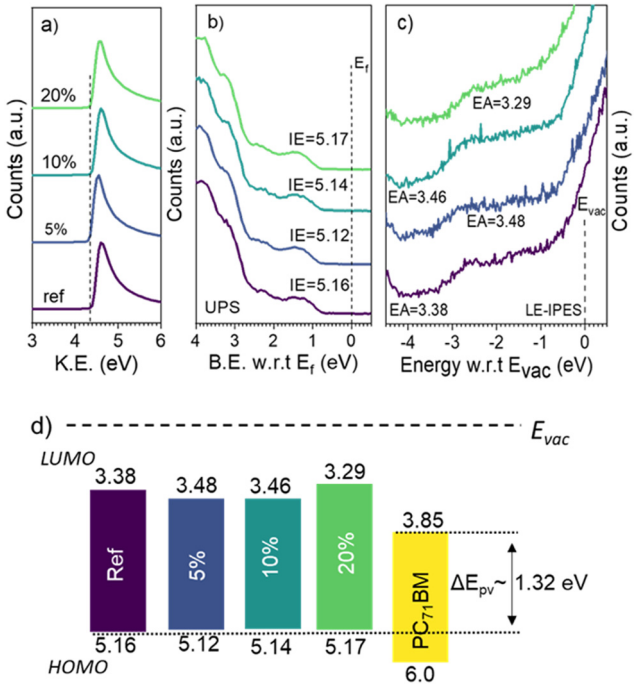

Fig. 3 (a and b) Ultraviolet photoelectron spectroscopy (UPS), (c) low-energy inverse photoelectron spectroscopy (LE-IPES) spectra of PDPP-TT polymer analogs, and (d) schematic depicting the measured frontier molecular orbital energies of PDPP-TT polymer analogs and the resultant photovoltaic gap (ΔE_{pv}).

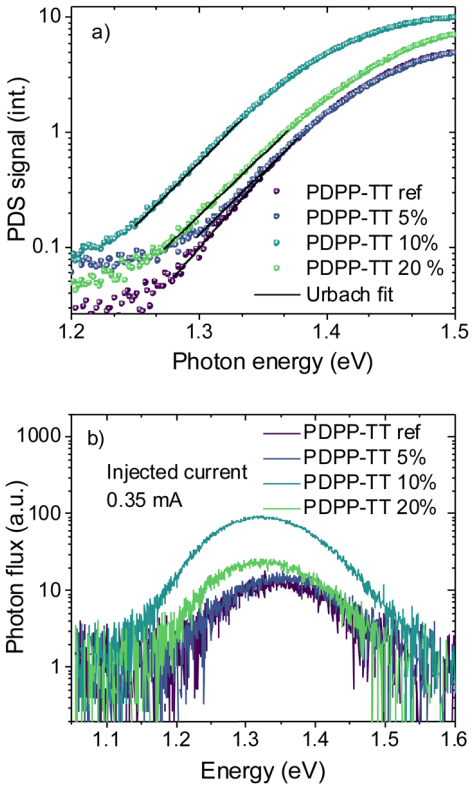

Fig. 4 (a) Photothermal deflection spectroscopy (PDS) spectra of polymer-$PC_{71}BM$ BHJ blend films, (b) electroluminescence (EL) spectra (uncorrected for detector sensitivity) measured at the same exposure time, of OSCs based on BHJ blends having various PDPP-TT polymer analogs with varying amounts of encapsulated units in the polymer backbone.

measured. When molecular encapsulation was introduced in the polymer backbone, E_u of all BHJ blends increased relative to the PDPP-TTref blend. E_u of BHJ blends based on PDPP-TT5%, PDPP-TT10%, and PDPP-TT20% polymers were found to be 40.33 ± 0.44 meV, 38.90 ± 0.22 meV, and 40.91 ± 0.26 meV, respectively, which are similar within the experimental uncertainties. Since the E_u reflects the structural disorder,[31] relatively higher E_u of BHJ blends with encapsulated polymers compared to the reference polymer shows that the molecular encapsulation in the polymer backbone results in increased structural disorder.

This interpretation is further supported by electroluminescence (EL) measurements performed to study the changes in the emissivity of polymers when encapsulated. Fig. 4b shows the spectra of devices measured at a fixed injection current of 0.35 mA with different PDPP-TT polymer analogs. The EL intensity of the device based on PDPP-TT10% was found to be about an order of magnitude higher at a fixed injection current density of 3.5 mA cm^{-2}, as compared to that in the case of PDPP-TTref devices. This demonstrates that the molecular encapsulation in the polymer backbone leads to higher emissivity by limiting the formation of non-radiative quenching sites, and recombination in such devices is more radiative in nature. Interestingly, when encapsulation was further increased to 20%, the EL intensity was reduced again, identifying PDPP-TT10% devices to be the most emissive. This is in agreement with the photovoltaic parameters of devices, which show that PDPP-TT10% results in OSCs with the highest V_{oc}, and a relatively lower V_{oc} is observed in the case of PDPP-TT20% devices.

To obtain further insight into the V_{oc} enhancement with molecular encapsulation in the polymer backbone, we evaluated the radiative and non-radiative energy loss. The $E_{g\,opt}$ of the PDPP-TTref and PDPP-TT5% devices, determined as per the reported procedure,[32] from the derivative of EQE spectra of the fully functional devices was found to be 1.43 eV. For PDPP-TT10% and PDPP-TT20% devices, an $E_{g\,opt}$ of 1.42 eV was measured. This agrees with the nearly unchanged IE of the PDPP-TT polymer analogs with varying amounts of encapsulated units (Fig. 3b). Utilizing the measured $E_{g\,opt}$ and the V_{oc} of devices, ΔE_{loss} was calculated to be 0.79 V for PDPP-TTref and PDPP-TT5% devices, whereas it was 0.73 V for PDPP-TT10% and 0.77 V for the PDPP-TT20% devices, respectively.

The radiative limit (ΔV_{ocrad}) and the (ΔV_{ocnr}) was calculated by using the relation expressed in eqn (3)–(5),[33] where the reconstructed EQE_{pv} from blackbody (Φ_{BB}) corrected EL spectrum was combined with the EQE spectrum (Fig. S19b, ESI†) to enhance the resolution of the measurements.[4] In eqn (3), $J_{0,rad}$ represents the current density simulating the blackbody radiation of the device at room temperature, k_B is the Boltzmann's constant, E is the photon energy, and T is 300 K.

$$J_{0,\mathrm{rad}} = -q\int_0^\infty \mathrm{EQE}_{\mathrm{pv}}(E)\cdot\Phi_{\mathrm{BB}}(E)\mathrm{d}E \qquad (3)$$

$$V_{\mathrm{ocrad}} = \frac{k_B T}{q} \ln\left(\frac{J_{\mathrm{sc}}}{J_{0,\mathrm{rad}}} + 1\right) \quad (4)$$

$$\Delta V_{\mathrm{ocnr}} = V_{\mathrm{ocrad}} - V_{\mathrm{oc}} \quad (5)$$

(ΔV_{ocnr}) for the PDPP-TTref and PDPP-TT5% devices were calculated to be 0.41 V (Table 2). In the case of PDPP-TT10%, (ΔV_{ocnr}) of 0.35 V, $\sim$ 60 mV lower than the reference device was measured. For PDPP-TT20%, (ΔV_{ocnr}) was evaluated to be 0.38 V, 30 mV higher than that in PDPP-TT10% devices, and is in agreement with the higher V_{oc} and enhanced emissivity observed with the PDPP-TT10% devices. This demonstrates that the introduction of molecular encapsulation in the polymer backbone is an effective strategy to reduce(ΔV_{ocnr}) in devices by making encapsulated polymers intrinsically more emissive, at the expense of increased structural disorder.

Lastly, morphology characterizations were performed to directly probe the morphological changes upon molecular encapsulation. The surface topographical images of polymer thin films from atomic force microscopy (AFM) show domains with fibrillar structures of polymer chains for PDPP-TTref (Fig. S21a, ESI†). Upon introducing the encapsulated units within the polymer backbone, the fibrillar structures were slightly suppressed for PDPP-TT5%. The fibrillar structures were not evident within the experimental resolution for the PDPP-TT10% and PDPP-TT20%, which show lobular domains. The thin film surface topography of all four polymer analogs, when mixed with [6,6]phenylC_{71}-butric acid methyl ester ($PC_{71}BM$) in a BHJ blend, was largely consistent with that found for neat polymers. PDPP-TTref and PDPP-TT5% blends with $PC_{71}BM$ displayed molecular aggregates with fibrillar structures, which were subsequently suppressed for BHJ blends of PDPP-TT10% and PDPP-TT20% (Fig. S21b, ESI†).

Grazing-incidence X-ray diffraction (GIXRD) analysis (Fig. 5) of the BHJ blend films shows prominent 100 and 200 peaks for the PDPP-TTref:$PC_{71}BM$ BHJ, owed to the lamellar stacking of the PDPP-TTref polymer, along with isotropic rings corresponding to the packing of $PC_{71}BM$ (Fig. 5). The introduction of the encapsulation (PDPP-TT5%) led to a reduction of the *d*-spacing of the lamellar stacking of the 100 and 200 reflections (Table S5, ESI†). Additionally, the area of both peaks reduces, suggesting a lower crystallinity of this DPP polymer. Finally, both polymers PDPP-TT10%, and PDPP-TT20% show no prominent lamellar reflections (Fig. 5c and d, respectively), further confirming the suppression of the molecular packing with the introduction of encapsulation into the polymer backbone. The reduced molecular order in the BHJ films upon encapsulation agrees with the observed enhancement in V_{oc}.[34]

Changes in the morphology and crystallinity or molecular ordering in polymer thin films often correlate with changes in the thermal[35,36] and carrier transport characteristics.[37] The charge carrier mobility of all PDPP-TT polymer analogs was thus measured using an organic field-effect transistor (OFET) with a bottom contact-top gate configuration. The OFET demonstrated dominant hole transport characteristics with high linear mobility (μ_{lin}) of 0.5 $cm^2\ V^{-1}\ S^{-1}$ for PDPP-TTref (Fig. S22, ESI†), comparable to that reported earlier.[21] However, with molecular

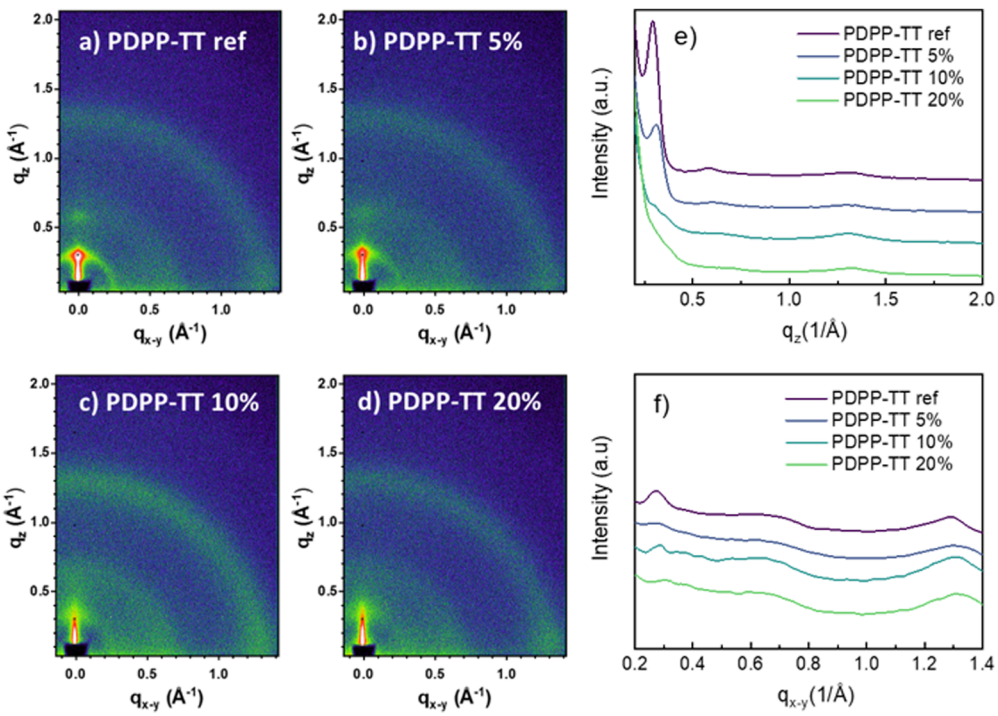

Fig. 5 2D-GIXRD profiles of polymer-$PC_{71}BM$ BHJ films with DPP polymer analogs (a) PDPP-TTref, (b) PDPP-TT5%, PDPP-TT10%, and PDPP-TT20%, (e) and (f) show the respective line-cuts.

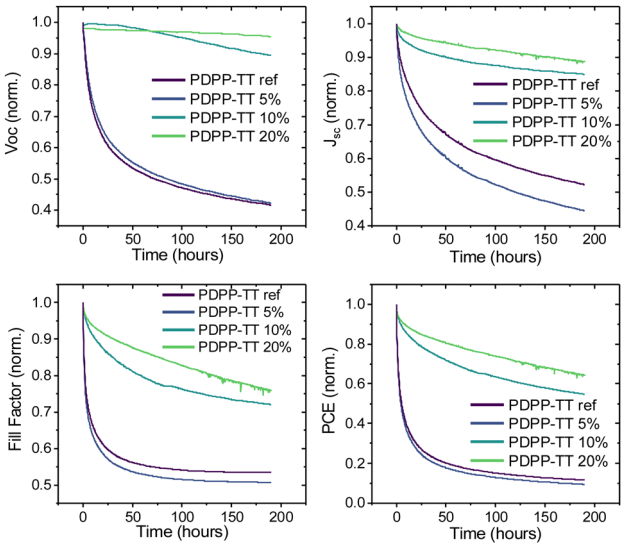

Fig. 6 Photostability of polymer-$PC_{71}BM$ BHJ OSCs incorporating different PDPP-TT polymer analogs with varying amounts of molecular encapsulation as donor material.

encapsulation in the polymer backbone, μ_{lin} was found to systematically decrease with an increasing number of encapsulated units in the backbone, resulting in μ_{lin} of 0.35 $cm^2\ V^{-1}\ S^{-1}$, 0.18 $cm^2\ V^{-1}\ S^{-1}$ and 0.03 $cm^2\ V^{-1}\ S^{-1}$ for PDPP-TT5%, PDPP-TT10%, and PDPP-TT20%, respectively. A similar trend was observed for the saturation mobility (μ_{sat}), where increasing the ratio of encapsulated units in the polymer backbone results in a systematic decrease of μ_{sat}. Lower charge mobility with molecular encapsulation in the polymer backbone confirms that the introduction of encapsulated units in the polymer backbone decreases the molecular packing between adjacent polymer chains, resulting in reduced molecular order in thin polymer films. Interestingly, the threshold voltage (V_{th}) is also reduced in the case of encapsulated polymer analogs. PDPP-TTref shows V_{th} = 49.8 V, which is decreased to 26.7 V for PDPP-TT10%, suggesting a reduction in the trap density.[38] Finally, PDPP-TT20% shows V_{th} of 54.3 V, suggesting a higher trap density. These results are in good agreement with the intensity-dependent V_{oc} measurements, where PDPP-TT10% shows the lowest trap-assisted recombination. Even though FET-measured mobility is not directly relevant for understanding the properties of solar cells as FET characterizes the charge transport parallel to the substrate, it provides useful insights into the morphology of polymer films after encapsulation. Nevertheless, the observed changes in mobility and trap-assisted recombination in OSCs are in agreement.

Finally, the photostability of OSCs based on different PDPP-TT polymer analogs was studied. Devices based on the PDPP-TTref and PDPP-TT5% polymers had significant burn-in losses, losing almost 80% of PCE in the first 25 h of operation with all device parameters undergoing severe degradation (Fig. 6). On the contrary, the PDPP-TT10% and PDPP-TT20% devices were relatively more stable, retaining almost 50% of the initial PCE after up to 200 h of operation. The significant enhancement in photostability of PDPP-TT10% and PDPP-TT20% devices is largely due to the negligible change in the V_{oc} during the initial burn-in period of up to 25 h. This suggests that the increased intermixing of the polymer and $PC_{71}BM$ phases in the case of PDPP-TT10% and PDPP-TT20% devices result in more stable BHJ morphology, ensuring more resilient devices under operation. This strategy can be extended further to other π-conjugated systems and utilized as a new strategy to extend the lifetime of OPV devices.

Conclusion

In conclusion, a series of low-bandgap encapsulated DPP-based polymers were synthesized using molecular encapsulation. The encapsulated material design enhanced the electroluminescence in OSCs *via* suppressed intramolecular aggregation, resulting in a notable reduction of non-radiative voltage losses. OSCs based on the encapsulated polymers demonstrated reduced trap-assisted charge recombination and improved V_{oc} (~50 mV). Moreover, molecular encapsulation led to a significant enhancement in the OSC photo-stability *via* better control over the D–A morphology. The implications of the molecular encapsulation strategy presented in this work are highly relevant for designing high-performing π-conjugated materials and solar cells with high operational stability.

Experimental

UV-visible absorption spectroscopy

UV-vis absorption spectra of encapsulated PDPP-TT polymer analogs were measured either in solution with chlorobenzene (CB) as the solvent or on thin films deposited from CB solution (5 mg mL^{-1}) on a glass substrate.

OSC Fabrication and Testing

OSCs were fabricated with the structure ITO/PEDOT:PSS (20 nm)/BHJ active layer (~100 nm)/DPO (~6 nm)/Ag (80 nm). ITO (10 Ω sq^{-1}) was cleaned by ultrasonication in a 2% aqueous solution of glass detergent (Hellmanex TM III) for 10 minutes before rinsing in DI water. ITO substrates were subsequently ultrasonicated in DI water, acetone, and isopropyl alcohol (IPA) for 10 minutes each, before cleaning in oxygen plasma for 10 minutes. PEDOT:PSS (CLEVIOS P VP AI 4083) was then spin-coated at 4000 rpm for 40 seconds, and the substrates were then annealed at 160 °C for 10 minutes in the air before transferring the substrates to the glove box. The active layer was deposited from a polymer: PC71BM (1 : 3) BHJ solution in chlorobenzene with 3% diphenyl ether as the solvent additive. DPO (0.5 mg mL^{-1} in IPA) was spin-coated at 2000 rpm for 20 seconds to result in a ~6 nm ETL before thermally evaporating a 100 nm silver electrode. The active area of all devices, as defined by the electrode geometry, was 0.1 cm^{-2}. Average PCE values were calculated from an average of at least six devices.

The photovoltaic characteristics of devices were measured in a nitrogen-filled glove box with a Keithly 2400 source meter and an Orial Sol3A Class AAA solar simulator with an AM1.5 filter and calibrated to 1 sun using a Newport certified KG-5 silicon

reference cell. External quantum efficiency (EQE) measurements were performed using an integrated system with a xenon arch lamp from Enlitech, Taiwan.

Ultraviolet photoelectron spectroscopy (UPS) and low-energy inverse photoelectron spectroscopy (LE-IPES)

The ionization energy (IE) and electron affinity (EA) of polymers were measured using UPS and LE-IPES, as described elsewhere.[39] Briefly, the polymer thin films were deposited on Au-coated Si substrates by spin-coating polymer solution (2 mg mL^{-1} in chlorobenzene) at 2500 rpm. UPS measurements were performed in an ultrahigh vacuum chamber with a base pressure of 10–10 mbar, equipped with a 7-channel hemispherical analyzer (Sphera II EAC 125), calibrated with the Fermi edge of polycrystalline silver. The measurements were performed at a pass energy of 10 eV using He 1 line with excitation energy of 21.22 eV. The estimated precision and spectral reproducibility in UPS measurements was $\pm$0.05 eV. LE-IPES measurements were performed in isochromatic mode (base pressure 10^{-9} mbar) using a PMT detector (Hamamatsu R585) mounted with a 280 nm filter (10 nm wavelength window) and an in-house build setup. The onset energies of the unoccupied molecular orbitals were estimated by deconvoluting the spectra using a Gaussian function and a Tougaard background, with an estimated uncertainty of $\pm$0.1 eV.

Electroluminescence (EL)

EL spectra were measured on best devices inside a nitrogen-filled glove box either by applying a DC voltage to the device equal to the V_{oc} at one sun illumination or at a fixed injection current of 0.35 mA (3.5 mA cm^{-2}). The emission collected by a collimator reached the spectrograph (Princeton Instruments SP-2300) through an optical fiber. The Pix100BRX Si detector was wavelength calibrated using a Ne/Ar light source (Princeton Instruments Intellical). The EL spectra measured using the Si detector were corrected for detector sensitivity to calculate the (ΔV_{ocnr}).

Sensitive EQE (sEQE)

sEQE measurements were performed at short-circuit under focused illumination from xenon arch lamp. The light beam was modulated by an optical chopper (275 Hz). The photocurrent was measured as a function of incident photon energy using a lock-in amplifier (Stanford Instruments SR830, and the lamp intensity was calibrated using a Si photodiode. The EL spectra (corrected for detector sensitivity) were used to reconstruct the EQEpv spectra at low photon energies according to the reciprocity relation.[4]

Photothermal deflection spectroscopy (PDS)

PDS measurements were performed on thin polymer: PC71BM (1 : 3) blend films (20 mg mL^{-1} in chlorobenzene with 3% diphenyl ether as solvent additive) spin-coated on Quartz using a home-built PDS setup. The light from a 250 W quartz tungsten-halogen lamp (Newport 66996-250Q-R1) was sent through a monochromator (LOT MSH-300) and used as a pump allowing excitation across the UV-to-near-infrared spectral region. The pump light was modulated by a chopper operating at a constant frequency of a few hertz (4 Hz for the present case) and focused on the sample, which was immersed in a chemically inert liquid [perfluorohexane (C6F14); Sigma-Aldrich] during the measurement. A small fraction of the monochromatic pump light was split off as intensity reference and measured by lock-in detection (Stanford Research Systems SR830 lock-in amplifier) using a pyroelectric detector (Newport DET-L-PYC5-R-P). Thin-film samples for PDS were prepared on cleaned quartz substrates by spin coating the polymer: PC71BM BHJ solution (20 mg mL^{-1} in chlorobenzene). A stabilized continuous-wave laser (Thorlabs HRS015 HeNe, 633 nm) was used as a probe beam source focused closely on the sample surface. The deviation of the probe beam was detected by a Si quadrant detector (Thorlabs PDP90A) using lock-in detection (Stanford Research Systems SR830). The entire setup was controlled by a home-built LabVIEW-based data acquisition and device control code. Further details can be found in the ESI.†

Author contributions

A. S.: conceptualization, data curation and analysis, methodology, investigation, project management, and writing the original draft. L. S.: polymer synthesis and characterization, writing – review & editing. J. B.: investigation, D. R. V.: mobility and morphology characterization; Y. G.: PDS measurements; C. D. C. and J. G.: writing – review & editing; J. T.: stability measurements; F. L.: resources, writing – review & editing; H. B. and D. B.: resources, conceptualization, funding acquisition, writing – review & editing.

Conflicts of interest

There are no conflicts to declare.

Acknowledgements

This work was supported by King Abdullah University of Science and Technology (KAUST) Office of Sponsored Research under award no. OSR-CARF/CCF-3079, OSR-CRG2018-3737, OSR-CRG2018-3746, and OSR-CRG2019-4025. HB acknowledges the support from Engineering and Physical Sciences Research Council (EPSRC) under award no. EP/S003126/1.

References

1 O. Inganas, Organic Photovoltaics over Three Decades, *Adv. Mater.*, 2018, **30**, e1800388.
2 C. Li, J. Zhou, J. Song, J. Xu, H. Zhang, X. Zhang, J. Guo, L. Zhu, D. Wei, G. Han, J. Min, Y. Zhang, Z. Xie, Y. Yi, H. Yan, F. Gao, F. Liu and Y. Sun, Non-fullerene acceptors with branched side chains and improved molecular packing to exceed 18% efficiency in organic solar cells, *Nat. Energy*, 2021, **6**, 605–613.
3 Y. Cui, Y. Xu, H. Yao, P. Bi, L. Hong, J. Zhang, Y. Zu, T. Zhang, J. Qin, J. Ren, Z. Chen, C. He, X. Hao, Z. Wei

and J. Hou, Single-Junction Organic Photovoltaic Cell with 19% Efficiency, *Adv. Mater.*, 2021, **33**, 2102420.
4 U. Rau, Reciprocity relation between photovoltaic quantum efficiency and electroluminescent emission of solar cells, *Phys. Rev. B: Condens. Matter Mater. Phys.*, 2007, **76**, 085303.
5 W. Shockley and H. J. Queisser, Detailed Balance Limit of Efficiency of p–n Junction Solar Cells, *J. Appl. Phys.*, 1961, **32**, 510–519.
6 M. A. Green, Radiative efficiency of state-of-the-art photovoltaic cells, *Prog. Photovoltaics*, 2012, **20**, 472–476.
7 K. D. Rosenthal, M. P. Hughes, B. R. Luginbuhl, N. A. Ran, A. Karki, S.-J. Ko, H. Hu, M. Wang, H. Ade and T.-Q. Nguyen, Quantifying and Understanding Voltage Losses Due to Nonradiative Recombination in Bulk Heterojunction Organic Solar Cells with Low Energetic Offsets, *Adv. Energy Mater.*, 2019, **9**, 1901077.
8 X. Liu, X. Du, J. Wang, C. Duan, X. Tang, T. Heumueller, G. Liu, Y. Li, Z. Wang, J. Wang, F. Liu, N. Li, C. J. Brabec, F. Huang and Y. Cao, Efficient Organic Solar Cells with Extremely High Open-Circuit Voltages and Low Voltage Losses by Suppressing Nonradiative Recombination Losses, *Adv. Energy Mater.*, 2018, **8**, 1801699.
9 X.-K. Chen and J.-L. Brédas, Voltage Losses in Organic Solar Cells: Understanding the Contributions of Intramolecular Vibrations to Nonradiative Recombinations, *Adv. Energy Mater.*, 2018, **8**, 1702227.
10 D. Qian, Z. Zheng, H. Yao, W. Tress, T. R. Hopper, S. Chen, S. Li, J. Liu, S. Chen, J. Zhang, X. K. Liu, B. Gao, L. Ouyang, Y. Jin, G. Pozina, I. A. Buyanova, W. M. Chen, O. Inganas, V. Coropceanu, J. L. Bredas, H. Yan, J. Hou, F. Zhang, A. A. Bakulin and F. Gao, Design rules for minimizing voltage losses in high-efficiency organic solar cells, *Nat. Mater.*, 2018, **17**, 703–709.
11 O. D. Miller, E. Yablonovitch and S. R. Kurtz, Strong Internal and External Luminescence as Solar Cells Approach the Shockley-Queisser Limit, *IEEE J. Photovolt.*, 2012, **2**, 303–311.
12 X. K. Chen, D. P. Qian, Y. M. Wang, T. Kirchartz, W. Tress, H. F. Yao, J. Yuan, M. Hulsbeck, M. J. Zhang, Y. P. Zou, Y. M. Sun, Y. F. Li, J. H. Hou, O. Inganas, V. Coropceanu, J. L. Bredas and F. Gao, A unified description of non-radiative voltage losses in organic solar cells, *Nat. Energy*, 2021, **6**, 799–806.
13 S. Albrecht, S. Janietz, W. Schindler, J. Frisch, J. Kurpiers, J. Kniepert, S. Inal, P. Pingel, K. Fostiropoulos, N. Koch and D. Neher, Fluorinated Copolymer PCPDTBT with Enhanced Open-Circuit Voltage and Reduced Recombination for Highly Efficient Polymer Solar Cells, *J. Am. Chem. Soc.*, 2012, **134**, 14932–14944.
14 J. Bertrandie, J. Han, C. S. P. De Castro, E. Yengel, J. Gorenflot, T. Anthopoulos, F. Laquai, A. Sharma and D. Baran, The Energy Level Conundrum of Organic Semiconductors in Solar Cells, *Adv. Mater.*, 2022, **34**, e2202575.
15 S. Karuthedath, J. Gorenflot, Y. Firdaus, N. Chaturvedi, C. S. P. De Castro, G. T. Harrison, J. I. Khan, A. Markina, A. H. Balawi, T. A. D. Peña, W. Liu, R.-Z. Liang, A. Sharma, S. H. K. Paleti, W. Zhang, Y. Lin, E. Alarousu, D. H. Anjum, P. M. Beaujuge, S. De Wolf, I. McCulloch, T. D. Anthopoulos, D. Baran, D. Andrienko and F. Laquai, Intrinsic efficiency limits in low-bandgap non-fullerene acceptor organic solar cells, *Nat. Mater.*, 2021, **20**, 378–384.
16 A. Classen, C. L. Chochos, L. Lüer, V. G. Gregoriou, J. Wortmann, A. Osvet, K. Forberich, I. McCulloch, T. Heumüller and C. J. Brabec, The role of exciton lifetime for charge generation in organic solar cells at negligible energy-level offsets, *Nat. Energy*, 2020, **5**, 711–719.
17 Q. Liu, S. E. Bottle and P. Sonar, Developments of Diketopyrrolopyrrole-Dye-Based Organic Semiconductors for a Wide Range of Applications in Electronics, *Adv. Mater.*, 2020, **32**, 1903882.
18 W. Li, K. H. Hendriks, A. Furlan, W. S. C. Roelofs, S. C. J. Meskers, M. M. Wienk and R. A. J. Janssen, Effect of the Fibrillar Microstructure on the Efficiency of High Molecular Weight Diketopyrrolopyrrole-Based Polymer Solar Cells, *Adv. Mater.*, 2014, **26**, 1565–1570.
19 Z. Hu, A. P. Willard, R. J. Ono, C. W. Bielawski, P. J. Rossky and D. A. Vanden Bout, An insight into non-emissive excited states in conjugated polymers, *Nat. Commun.*, 2015, **6**, 8246.
20 J. Wang, X. Jiang, H. Wu, G. Feng, H. Wu, J. Li, Y. Yi, X. Feng, Z. Ma, W. Li, K. Vandewal and Z. Tang, Increasing donor-acceptor spacing for reduced voltage loss in organic solar cells, *Nat. Commun.*, 2021, **12**, 6679.
21 K. Sugiyasu, Y. Honsho, R. M. Harrison, A. Sato, T. Yasuda, S. Seki and M. Takeuchi, A Self-Threading Polythiophene: Defect-Free Insulated Molecular Wires Endowed with Long Effective Conjugation Length, *J. Am. Chem. Soc.*, 2010, **132**, 14754–14756.
22 C. Pan, K. Sugiyasu, Y. Wakayama, A. Sato and M. Takeuchi, Thermoplastic Fluorescent Conjugated Polymers: Benefits of Preventing π–π Stacking, *Angew. Chem., Int. Ed.*, 2013, **52**, 10775–10779.
23 A. Leventis, J. Royakkers, A. G. Rapidis, N. Goodeal, M. K. Corpinot, J. M. Frost, D.-K. Bučar, M. O. Blunt, F. Cacialli and H. Bronstein, Highly Luminescent Encapsulated Narrow Bandgap Polymers Based on Diketopyrrolopyrrole, *J. Am. Chem. Soc.*, 2018, **140**, 1622–1626.
24 W. W. Li, K. H. Hendriks, W. S. C. Roelofs, Y. Kim, M. M. Wienk and R. A. J. Janssen, Efficient Small Bandgap Polymer Solar Cells with High Fill Factors for 300 nm Thick Films, *Adv. Mater.*, 2013, **25**, 3182–3186.
25 H. Bronstein, Z. Chen, R. S. Ashraf, W. Zhang, J. Du, J. R. Durrant, P. Shakya Tuladhar, K. Song, S. E. Watkins, Y. Geerts, M. M. Wienk, R. A. J. Janssen, T. Anthopoulos, H. Sirringhaus, M. Heeney and I. McCulloch, Thieno[3,2-b]thiophene−Diketopyrrolopyrrole-Containing Polymers for High-Performance Organic Field-Effect Transistors and Organic Photovoltaic Devices, *J. Am. Chem. Soc.*, 2011, **133**, 3272–3275.
26 Deposition numbers CCDC 2164409 (for 2), and CCDC 2177219 (for 3) contain the supplementary crystallographic data for this paper. These data are provided free of charge by the joint Cambridge Crystallographic Data Centre and

Fachinformationszentrum Karlsruhe Access Structures service.

27 H. Choi, S.-J. Ko, T. Kim, P.-O. Morin, B. Walker, B. H. Lee, M. Leclerc, J. Y. Kim and A. J. Heeger, Small-Bandgap Polymer Solar Cells with Unprecedented Short-Circuit Current Density and High Fill Factor, *Adv. Mater.*, 2015, **27**, 3318–3324.

28 P. Schilinsky, C. Waldauf and C. J. Brabec, Recombination and loss analysis in polythiophene based bulk heterojunction photodetectors, *Appl. Phys. Lett.*, 2002, **81**, 3885–3887.

29 K. Vandewal, J. Widmer, T. Heumueller, C. J. Brabec, M. D. McGehee, K. Leo, M. Riede and A. Salleo, Increased Open-Circuit Voltage of Organic Solar Cells by Reduced Donor-Acceptor Interface Area, *Adv. Mater.*, 2014, **26**, 3839–3843.

30 Y. Gao, K. Wang, M. Wang, J. I. Khan, A. H. Balawi, W. Liu, S. De Wolf and F. Laquai, Impact of Cesium/Rubidium Incorporation on the Photophysics of Multiple-Cation Lead Halide Perovskites, *Solar RRL*, 2020, **4**, 2000072.

31 C. Kaiser, O. J. Sandberg, N. Zarrabi, W. Li, P. Meredith and A. Armin, A universal Urbach rule for disordered organic semiconductors, *Nat. Commun.*, 2021, **12**, 3988.

32 U. Rau, B. Blank, T. C. M. Muller and T. Kirchartz, Efficiency Potential of Photovoltaic Materials and Devices Unveiled by Detailed-Balance Analysis, *Phys. Rev. Appl.*, 2017, **7**, 044016.

33 M. Azzouzi, J. Yan, T. Kirchartz, K. Liu, J. Wang, H. Wu and J. Nelson, Nonradiative Energy Losses in Bulk-Heterojunction Organic Photovoltaics, *Phys. Rev. X*, 2018, **8**, 031055.

34 F. Piersimoni, S. Chambon, K. Vandewal, R. Mens, T. Boonen, A. Gadisa, M. Izquierdo, S. Filippone, B. Ruttens, J. D'Haen, N. Martin, L. Lutsen, D. Vanderzande, P. Adriaensens and J. V. Manca, Influence of Fullerene Ordering on the Energy of the Charge-Transfer State and Open-Circuit Voltage in Polymer:Fullerene Solar Cells, *J. Phys. Chem. C*, 2011, **115**, 10873–10880.

35 A. Sharma, X. Pan, J. A. Campbell, M. R. Andersson and D. A. Lewis, Unravelling the Thermomechanical Properties of Bulk Heterojunction Blends in Polymer Solar Cells, *Macromolecules*, 2017, **50**, 3347–3354.

36 A. Sharma, X. Pan, J. M. Bjuggren, D. Gedefaw, X. Xu, R. Kroon, E. Wang, J. A. Campbell, D. A. Lewis and M. R. Andersson, Probing the Relationship between Molecular Structures, Thermal Transitions, and Morphology in Polymer Semiconductors Using a Woven Glass-Mesh-Based DMTA Technique, *Chem. Mater.*, 2019, **31**, 6740–6749.

37 R. Noriega, J. Rivnay, K. Vandewal, F. P. V. Koch, N. Stingelin, P. Smith, M. F. Toney and A. Salleo, A general relationship between disorder, aggregation and charge transport in conjugated polymers, *Nat. Mater.*, 2013, **12**, 1038.

38 S. Olthof, S. Singh, S. K. Mohapatra, S. Barlow, S. R. Marder, B. Kippelen and A. Kahn, Passivation of trap states in unpurified and purified C60 and the influence on organic field-effect transistor performance, *Appl. Phys. Lett.*, 2012, **101**, 253303.

39 A. Sharma, S. Singh, X. Song, D. Rosas Villalva, J. Troughton, D. Corzo, L. Toppare, G. Gunbas, B. C. Schroeder and D. Baran, A Nonionic Alcohol Soluble Polymer Cathode Interlayer Enables Efficient Organic and Perovskite Solar Cells, *Chem. Mater.*, 2021, **33**, 8602–8611.

